Surface Roughness Effects on Nosetip Ablation Characteristics

R. M. GRABOW* AND C. O. WHITE†
Aeronutronic Division of Philco-Ford Corporation, Newport Beach, Calif.

A model is presented for predicting the onset, growth rate, and geometric characteristics of surface roughness on re-entry vehicle nosetips. The roughness is characterized by scallop patterns, which are shown to be an advanced stage of ring waves or crosshatch patterns. The patterns act as time-variable surface roughness which augments the convective heating rates and alters nosetip ablation. The predicted geometry of the scallop patterns yields a roughness density parameter for evaluating the heating augmentation. The model has been incorporated into a nosetip recession and shape change computer program, and the results are shown to agree with experimental nosetip ablation data.

Nomenclature

A_p, A_s = projected area and surface area, respectively
C_D = roughness drag coefficient
$\bar{C}_i$ = imaginary part of complex wave velocity
C_f = skin friction coefficient
$E_{1,2}$ = material constants
K = pattern depth
M = Mach number
p = pressure
$\bar{P}_{\text{mag}}$ = amplitude of pressure perturbation $(p'_w/p_e)_{\text{mag}}/\gamma(\varepsilon/\delta)$
R_N = nosetip radius
R_{e_∞} = freestream unit Reynolds number, $\rho_\infty u_\infty/\mu_\infty$
R_{e_x} = Reynolds number at edge of boundary layer, $\rho_e u_e x/\mu_e$
R_{e_θ} = momentum thickness Reynolds number, $\rho_e u_e \theta/\mu_e$
t = time
T = temperature
u = velocity parallel to surface
x, y = Cartesian coordinates of surface
$\bar{\alpha}$ = dimensional wave number, $2\pi/\lambda_N$
γ = ratio of specific heats
δ = boundary-layer thickness
δ^* = boundary-layer displacement thickness
ε = amplitude of surface wave
θ = boundary-layer momentum thickness
θ_c = cone half angle
λ_L = wavelength in streamwise direction
λ_N = wavelength normal to wave crests
μ = gas viscosity
ρ = gas density
τ = shear stress
Φ_p = pressure phase angle

Subscripts

e = edge of boundary-layer value
mag = amplitude of perturbed quantity
N = normal to waves
o = stagnation value
s = sand roughness
w = wall value
∞ = freestream

Superscripts

$(\_)'$ = perturbation value
$(\bar{\ })$ = dimensional quantity
$*$ = reference temperature value

I. Introduction

THE nosetip of a re-entry vehicle generally experiences a severe aero-thermodynamic environment from the standpoint of loads, heating, and ablation. The presence of surface roughness can aggravate this condition by causing premature boundary-layer transition and subsequent increases in the shear stress, heating, and ablation rate distributions.

The nature of the surface roughness may be generally characterized as either "microscale" or "macroscale." The microscale roughness inherent in all materials is a measure of the characteristic grain size (typically in the range of 0.1–1.0 mil). This type of roughness has been shown[1] to have a significant effect on boundary-layer transition in the nosetip region. The premature occurrence of transition produces turbulent heating rates that are higher than the corresponding smooth wall laminar values. In addition, there is some augmentation of the turbulent heating due to the protrusion of the microscale roughness elements through the laminar sublayer. However, the most important effect to consider is that the turbulent flow triggered by the microscale roughness is capable of generating a large-scale macroscale roughness (typically in the range of 10–100 mils) which produces high augmentation of the turbulent heating rates. An example of macroscale roughness (scallop patterns) on

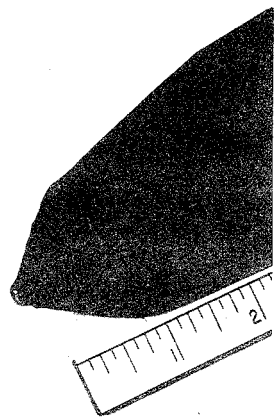

Fig. 1 Post test photograph of scallop patterns on graphite model.

Submitted June 14, 1974; presented as Paper 74-513 at the AIAA 7th Fluid and Plasma Dynamics Conference, Palo Alto, California; June 17–19, 1974; revision received October 21, 1974. This work was supported by Air Force Space and Missile Systems Organization, Contract F04701-72-C-0290.

Index categories: Supersonic and Hypersonic Flow; Material Ablation.

* Section Supervisor, Aero-thermodynamics. Member AIAA.
† Staff Member, Systems Engineering. Member AIAA.

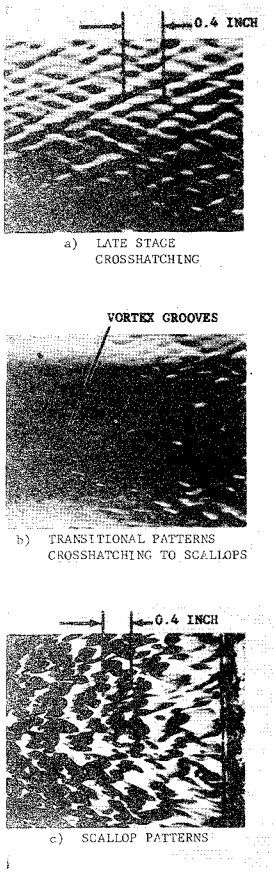

Fig. 2 Development of crosshatch patterns into scallop patterns.

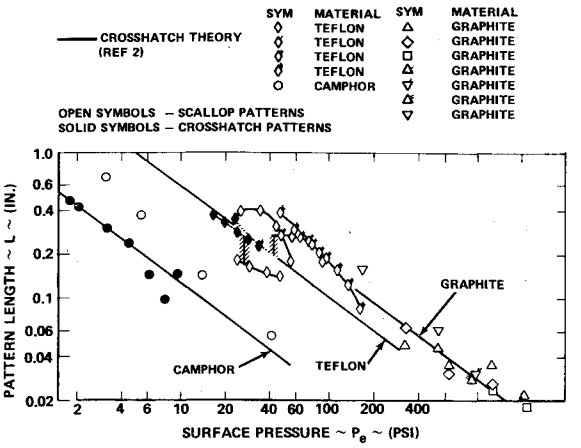

Fig. 3 Correlation of crosshatch and scallop pattern length.

a graphite nosetip exposed to a supersonic arc jet is shown in Fig. 1; it is this type of roughness that this paper is primarily concerned with.

II. Macroscale Roughness

The concept of turbulence-induced macroscale roughness stems from a model proposed by the authors in Ref. 2 for the development of surface crosshatch patterns. According to this model, the surface forms either a melt layer or viscoelastic layer which interacts with the turbulent boundary layer. A linear stability analysis is used to determine the conditions for which the disturbance motion is amplified, thereby resulting in surface wave onset and subsequent growth of the patterns. Depending on the magnitude of the amplification rate, the roughness depth increases with time until a point is reached when the crosshatch patterns degenerate into scallop patterns. This process is illustrated by the photographs shown in Fig. 2 for the case of a Teflon surface. For some materials, such as graphite, the degeneration to scallop patterns is so rapid that the initial crosshatch pattern is generally indiscernible. In addition, graphite nosetips most often show evidence of scallop patterns in regions where the flow is subsonic (see Fig. 1). For this condition, the model of Ref. 2 predicts two-dimensional ring waves; however, based on experimental observations, these waves also degenerate into scallop patterns early in the development stage.

The following sections address the ablating nosetip roughness problem with a view towards: 1) realistic-type roughness geometry, 2) heating augmentation factors that are appropriate for the expected type of roughness geometry and nosetip configurations, and 3) utilization of these factors in computer codes for predicting nosetip ablation and shape change.

III. Roughness Geometry

The geometric characteristics of scallop roughness patterns are found to be closely linked to the parent crosshatch or ring wave features. A detailed correlation of the similarities and deviations between the two types of patterns is presented in Ref. 3, and only a few salient features are provided here. Considering first the length dimension, Fig. 3 shows a comparison between the scallop length (L) and the corresponding crosshatch wavelengths (λ_L) for camphor, Teflon, and graphite materials. The dependence on pressure is shown to be similar for both types of patterns. It is noted that the theory of Ref. 2 predicted a dependence, $\lambda_L \sim P_e^{-0.7}$, while the experimental data indicate an exponent of -0.77.

Considering next the width dimension, Fig. 4 shows a correlation of the pattern length-to-width ration (L/W) as a function of local Mach number (M_e). This dependence is directly analogous to the similarity between the crosshatch wave angle and the local Mach angle.

The pattern depth is the most important geometric characteristic, and unfortunately, the most difficult to evaluate since it is time-dependent. Analytically, the pattern depth is computed from the relation

$$K = \int_o^{t_1} \bar{\alpha}\bar{C}_i K\, dt + K_1 \int_{t_i}^{t} \bar{\alpha}\bar{C}_i\, dt \qquad (1)$$

where the first integral term is the theoretically derived growth law[2] for the crosshatch regime, and utilizes the microscale roughness for the initial value of K. The integration limit (t_1) is the time when degeneration to scallops begins (from experimental results, this occurs when $K = K_1 = 0.04\lambda_L$). This behavior is graphically demonstrated in Fig. 5 for three camphor model wind tunnel tests.[4] The predicted pattern depth history is shown to be initially exponential, followed by a linear growth rate, in accordance with Eq. (1). The experimental data points in Fig. 5 are not intended to be measured pattern depths, rather, they represent the times at which the surface patterns were photographically observed to be of the groove, crosshatch, or scallop type. These data are shown to qualitatively support the premise

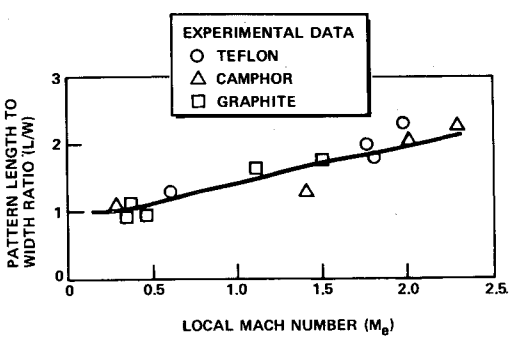

Fig. 4 Scallop length-to-width ratio.

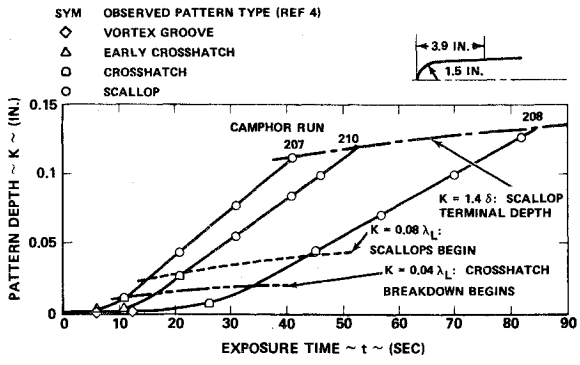

Fig. 5 Growth of patterns on camphor surface.

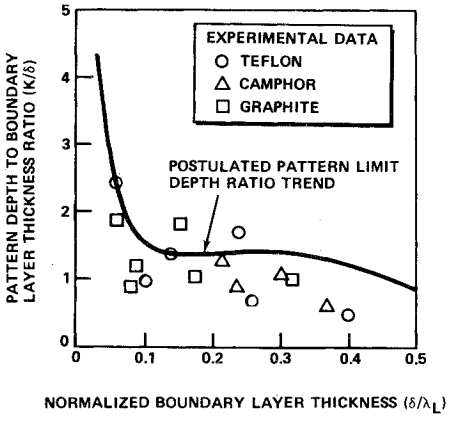

Fig. 7 Correlation of pattern terminal depth.

that the crosshatch patterns begin to degenerate to scallop patterns when the depth exceeds $0.04\lambda_L$.

The amplification rate is obtained from the relation derived in Ref. 2:

$$\bar{\alpha}\bar{C}_i = E_1 p_e \frac{\hat{P}_{\text{mag}} \cos\phi_p}{\delta/\lambda_N}\left[1 - \frac{E_2(T_W/1800)^{0.73}}{(p_e \tau_{w_N})^{1/3}\lambda_N^{2/3}}\right] \quad (2)$$

where the wavelength (λ_N) and shear stress (τ_{W_N}) are evaluated normal to the wave. The turbulent boundary-layer pressure perturbation is obtained from a combination of analytical results and wavy wall experimental data. For the case of thick turbulent boundary layers relative to the wavelength ($\delta/\lambda_N > 0.5$), the pressure perturbation has been correlated as a function of local Mach number normal to the waves (M_{e_N}), in the form

$$\frac{\hat{P}_{\text{mag}} \cos\phi_p}{\delta/\lambda_N} = \begin{cases} 3.33 M_{e_N}{}^2 & \text{for } M_{e_N} \leqq 1 \\ 3.33 & \text{for } M_{e_N} > 1 \end{cases} \quad (3)$$

Figure 6 presents a comparison between this result and the various experimental data. The two empirical material constants in Eq. (2) are given in Table 1 together with the critical surface temperature below which patterns will not occur. The amplification rate also serves as a criterion for pattern onset. If $\bar{\alpha}\bar{C}_i < 0$, macroscale roughness patterns are not predicted to occur. However, once the amplification rate becomes positive, the integration of Eq. (1) to obtain pattern depth proceeds to the point where the depth reaches a limiting value. From the correlation of Ref. 3, the limit depth is a function of smoothwall boundary-layer thickness (δ) and wavelength (λ_L), as shown in Fig. 7. For a large range of δ/λ_L, the limit depth is indicated to be 1.4 times the boundary-layer thickness. In the nosetip region where δ is small, the limit depth is reached rapidly, and scalloping occurs before crosshatching can fully develop.

Table 1 Critical surface temperature below which patterns will not occur

Material	E_1 (ft²/lb-sec)	E_2 (lb/ft)$^{2/3}$	$(T_W)_{\text{crit}}$ (°R)
Camphor	2×10^{-4}	0.68	600
Teflon	9×10^{-5}	1.77	950

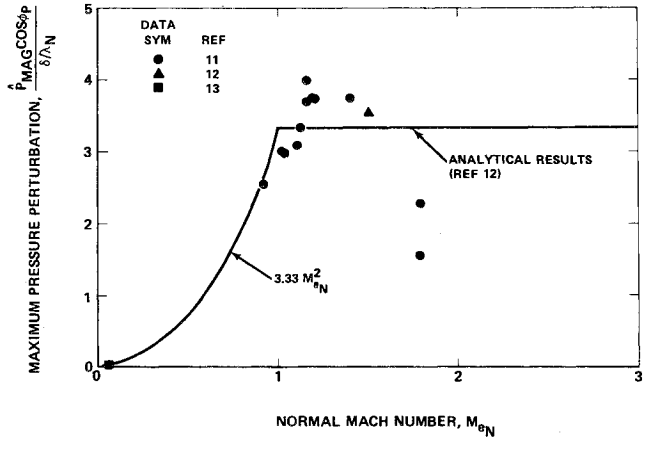

Fig. 6 Pressure perturbation parameter for turbulent flow over wavy surfaces.

IV. Heating Augmentation Factors

The surface roughness characteristics described in the preceding paragraph are used to define a roughness density parameter for correlating roughness efforts on heat transfer. According to the scheme developed in Ref. 5, the roughness density parameter is given by

$$\Lambda = (D/K)(A_s/A_p)^{4/3} \quad (4)$$

where A_s is the windward surface area of the roughness, A_p is the projected area of the roughness in the flow direction, and D is the inverse square root of the number of roughness elements per unit surface area. Defined in this manner, the roughness density parameter has been successfully used to correlate rough wall skin friction data (as derived from velocity profile measurements). The correlation of Ref. 5 (with additional

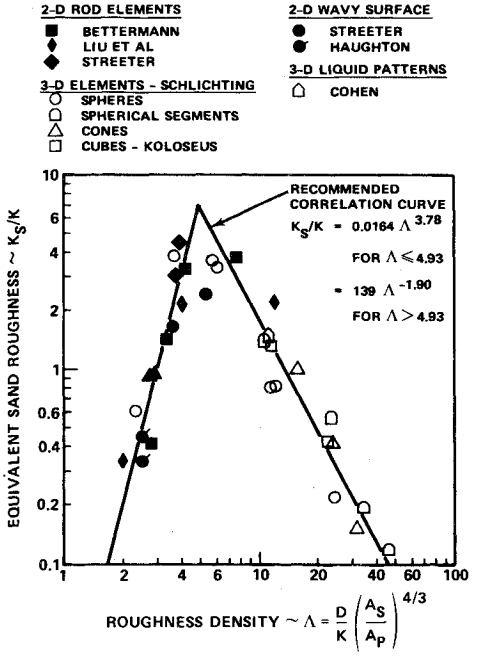

Fig. 8 Roughness density effect on equivalent sand roughness depth.

wavy wall and liquid pattern data points provided by the present authors) is presented in Fig. 8 as a ratio of equivalent sand roughness depth (K_s) to the actual roughness depth (K). These results indicate that a pattern configuration having a roughness density parameter of 4.93 will experience the largest skin friction increase (the equivalent sand roughness ratio being 7.0).

As indicated in Ref. 5, the area ratio (A_s/A_p) is actually a simplified representation of the roughness form drag. An equivalent parameter has been found to be the ratio of the roughness drag coefficient to the flat plate drag coefficient ($C_{D_{FP}}/C_D$), where $C_{D_{FP}} \simeq 1.3$ for a plate normal to the flow mounted on a planar surface. It can be shown that the experimental data of Fig. 8 correlate in the same manner in terms of the drag coefficient ratio. For these roughness elements, the drag coefficients are known reasonably well. However, for the scallop roughness patterns of interest to this study, the drag coefficients can only be speculated. Based on the observed cusp shapes of scallop profiles, it is believed that the drag coefficients are close to the flat plate value of 1.3. Thus, the drag ratio, or equivalently, the area ratio in Eq. (4), is assumed equal to unity. Further assuming that the patterns are rectangular, $D \simeq (L \times W)^{1/2}$, and the roughness density parameter may then be expressed in the simple form

$$\Lambda = (L/K)/(L/W)^{1/2} \tag{5}$$

From Fig. 4, the ratio (L/W) is approximately unity for subsonic flow conditions. If the roughness depth is 20% of the length (typical of scallop patterns), then $\Lambda \simeq 5$, which according to Fig. 6 results in a large equivalent sand roughness depth. Therefore, scallop patterns can experience larger skin friction increases than sand roughness of the same depth. The heat transfer will also be increased relative to the sand roughness case, but there is insufficient experimental data to quantify the dependence on roughness density. For this investigation, it will be assumed that the equivalent sand roughness correlation of Fig. 8 is also applicable to heat transfer data. This technique provides a means for employing heat transfer augmentation factors from sand roughened surfaces to predict heating augmentation on arbitrary roughened surfaces.

Various techniques have been developed for assessing the influence of sand roughness on turbulent heating augmentation. However, as shown in Ref. 3, there is significant disparity between these techniques, and no single approach agrees satisfactorily with the bulk of the experimental data (particularly for large roughness depths characteristic of scallop patterns). To improve this situation, the present authors developed a new correlation of experimental data that is applicable to large scale roughness on nosetips with strong flowfield gradients. The correlation is based on the work of Ref. 6 which utilizes the incompressible turbulent law of the wall to derive the rough-to-smooth skin friction ratio

$$\left(\frac{C_f}{C_{f_o}}\right)^{1/2} = (5.6 \log R_{e_\delta}{}^* + 4.8) \Big/ \left(5.6 \log \frac{\delta^*/K_s}{(C_{f_o}/2)^{1/2}} + 8.5\right) \tag{6}$$

where $R_{e_\delta}{}^*$ is the turbulent displacement thickness Reynolds number.

This relation suggests that $R_{e_\delta}{}^*$ and K_s/δ^* should be the primary parameters for correlating skin friction augmentation. It is further assumed that these same parameters can be used to correlate heat transfer augmentation, although the levels of augmentation are different for both quantities. Figure 9 shows the result of plotting the experimental heat transfer data from Refs. 7 and 8 in terms of the roughness ratio (K_s/δ^*). The free-stream Mach number is approximately 5, but the local Mach numbers vary from 0.5–2.0. There are also large Reynolds number variations, but the strong influence of $R_{e_\delta}{}^*$ indicated by Eq. (6) is not evident. The successful correlation in terms of K_s/δ^* indicates that this is the dominant parameter for evaluating roughness effects on heat transfer. It is noted that the turbulent displacement thicknesses (δ^*) are computed from the momentum-integral equation assuming a smooth surface skin friction law. Roughness effects tend to increase δ^*, but the present correlation does not attempt to account for this. The equations utilized for this purpose are[10]

$$\delta^* = \theta \left[1.3 \frac{T_w}{T_e} + \frac{T_o}{T_e} - 1\right] \tag{7}$$

where

$$\theta = \frac{0.0365x}{R_{e_x}{}^{0.2}} \left(\frac{\rho^*}{\rho_e}\right)^{0.8} \left(\frac{\mu^*}{\mu_e}\right)^{0.2} \left[\frac{\rho_e u_e{}^{2.25} \mu_e{}^{0.25} y^{1.25} x}{\int_o^x \rho_e u_e{}^{2.25} \mu_e{}^{0.25} y^{1.25}\, dx}\right]^{-0.8} \tag{8}$$

V. Nosetip Ablation Predictions

The scallop roughness methodology described in this paper has been implemented into the Philco-Ford Nosetip Recession and Shape Change (RASC) code. As described in Ref. 9, this code performs a coupled computation of the flow field, heating, ablation rate, and recession distributions for arbitrary shaped nosetips at zero or finite angle of attack. The following procedure is used to compute surface roughness effects:

1) Determine boundary-layer transition location on the basis of a momentum thickness Reynolds number (R_{e_θ}) that accounts for microscale roughness effects.

2) At all body stations downstream of the transition location, compute surface temperature, pressure, shear, Mach number, and amplification rate [Eq. (2)] to determine if scallop roughness patterns will occur.

3) If patterns occur, compute length, width, and depth using curve-fits of the results shown in Figs. 3–5, and the result of integrating Eq. (1). Terminal depth is obtained from Fig. 7.

4) Compute roughness density from Eq. (5), and use correlation of Fig. 8 to obtain the equivalent sand roughness height.

5) Compute the local turbulent boundary-layer displacement thickness from Eqs. (7) and (8), and utilize this quantity with the equivalent sand roughness height to obtain the rough-to-smooth heating ratio (performed with curve-fit to correlation of Fig. 9).

6) Utilize augmented heating rates to compute local ablation rates, and integrate with respect to time to obtain recession and overall nosetip shape change.

The RASC code has been used to predict nosetip ablation for a wide variety of materials (camphor, Teflon, graphite, and

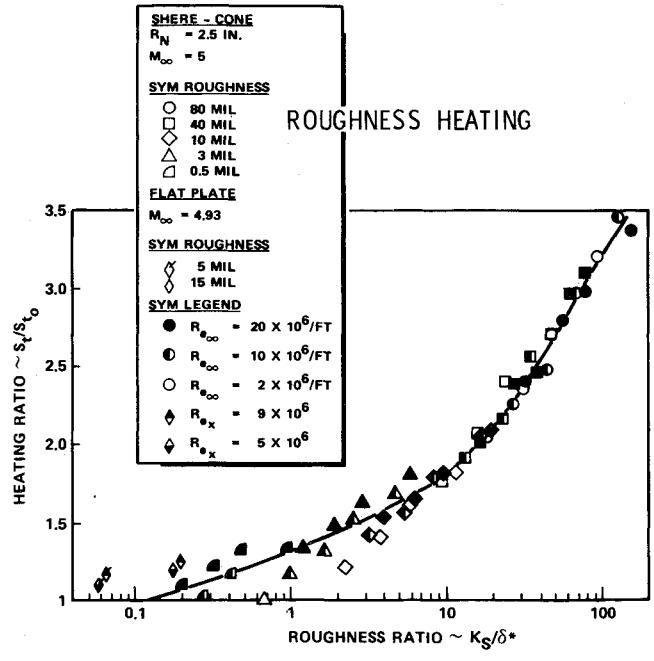

Fig. 9 Correlation of rough-to-smooth Stanton number ratio for sand-type roughness.

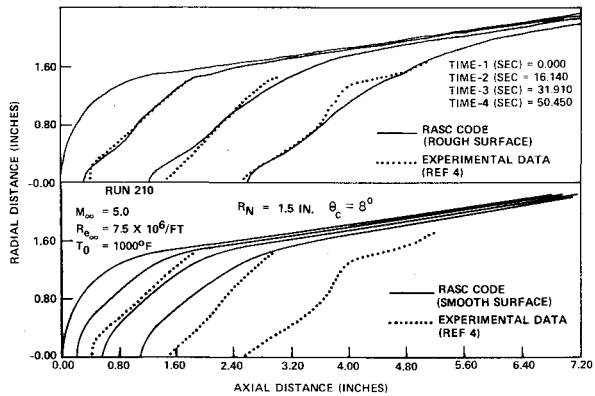

Fig. 10 Camphor nosetip ablation profiles; comparisons between data and predictions.

carbon composites) over a broad range of test conditions (wind tunnel, arc-jet, sounding rocket flight, and ballistic re-entry flight). For all cases where the computed amplification rate was finite ($\bar{\alpha}\bar{C}_i > 0$), it was necessary to include roughness augmented heating to obtain good agreement with measured ablation profiles. The neglect of roughness effects generally caused the total surface recession to be underpredicted by factors ranging between 1.5 and 2.5.

Recession and shape change predictions have been presented[14] for several camphor nosetip tested in a hypersonic wind tunnel.[4] For these conditions, boundary-layer transition was observed to occur at a location on the nosetip where the momentum thickness, $R_{e_\theta} \simeq 100$; therefore, this value was assumed to be a constant for all cases. Typical results for a 1.5 in. nose radius model are presented in Fig. 10.

The predictions made for a rough surface (accounting for scallop pattern development and augmentation heating) are shown to agree well with the data. However, the predictions for smooth surface heating rates significantly underpredict the recession. Since the transition location was the same for both computations, the differences are due entirely to macroroughness induced augmentation heating. It is noted that motion picture coverage of this test indicated crosshatch and scallop pattern development, as previously shown in Fig. 5. Similar results were obtained for other camphor models, and as shown in Ref. 14, the inclusion of roughness effects is essential to obtaining good agreement with measured ablation profiles.

VI. Conclusions

A method has been developed for evaluating surface roughness characteristics and heating augmentation factors for use in the prediction of nosetip ablation and shape change. The main conclusions of this study are: 1) The primary effect of microscale (grain-size) roughness is to influence the onset and progression of boundary-layer transition. 2) Macroscale roughness is postulated to be the result of a surface flow instability. The initial roughness is due to surface waves, which later degenerate into scallop patterns. 3) The roughness density parameter of Ref. 5 is an effective means of obtaining an equivalent sand roughness depth for correlating roughness effects on skin friction and heat transfer. 4) The influence of sand roughness on turbulent heat transfer is effectively correlated by the ratio of roughness depth to boundary layer displacement thickness. 5) Inclusion of scallop roughness effects in nosetip ablation codes has a large influence on computed nosetip recession and shape change. 6) Calculations performed for camphor nosetips tested in a wind tunnel indicate good agreement with measured recession and shape change data.

References

[1] Van Driest, E., Blumer, C., and Wells, C., "Boundary Layer Transition on Blunt Bodies—Effect of Roughness," *AIAA Journal*, Vol. 5, Oct. 1967, pp. 1913–1915.

[2] Grabow, R. and White, C., "A Surface Flow Approach for Predicting Crosshatch Patterns," *AIAA Journal*, Vol. 11, June 1973, pp. 841–847.

[3] White, C. and Grabow, R., "Influence of Scallop Roughness on Nosetip Shape Change Behavior," SAMSO TR73-88, Jan. 1973, Philco-Ford Corp., Newport Beach, Calif.

[4] Derbidge, T., Wool, M., and Baker, D., "PANT Series D Wind Tunnel Test Report," Aerotherm Project Rept. 7044, Jan. 1973, Aerotherm/Acurex Corp., Mountain View, Calif.

[5] Dirling, R., "A Method for Computing Roughwall Heat Transfer Rates on Re-Entry Nosetips," AIAA Paper 73-763, Palm Springs, Calif., 1973.

[6] Dvorak, F., "Calculation of Turbulent Boundary Layers on Rough Surfaces in Pressure Gradient," *AIAA Journal*, Vol. 7, Sept. 1969, pp. 1752–1759.

[7] Jackson, M., Baker, D., and Powars, C., "PANT Series A Wind Tunnel Test Report," Aerotherm Project Rept. 7042, Dec. 1972, Aerotherm/Acurex Corp., Mountain View, Calif.

[8] Young, F., "Experimental Investigation of the Effects of Surface Roughness on Compressible Turbulent Boundary Layer Skin Friction and Heat Transfer," DRL Rept.-532, May 1965, University of Texas, Austin, Texas.

[9] Grabow, R., "Recent Modifications to the Nosetip Recession and Shape Change Computer Code," DR 5706, Nov. 1973, Philco-Ford Corp., Newport Beach, Calif.

[10] Walker, G. and Schumann, B., "The Growth of Turbulent Boundary Layers," General Electric Technical Information Series, R615D123, July 1961, General Electric Co., Philadelphia, Pa.

[11] Williams, E. and Inger, G., "Investigations of Ablation Surface Crosshatching," SAMSO TN-70-246, June 1970, McDonnell-Douglas Corp., St. Louis, Mo.

[12] Conrad, P., Donaldson, DuP., and Snedeker, R., "A Study of the Modal Response Approach to Patterned Ablation, Including Experiment Definition," SAMSO TN-70-213, April 1970, Aeronautical Research Associates of Princeton, Princeton, N.J.

[13] Segal, A., "An Experimental Investigation of The Turbulent Boundary Layer Over a Wavy Wall," Ph.D. thesis, April 1971, Dept. of Aeronautics, California Institute of Technology, Pasadena, Calif.

[14] Grabow, R. and White, C., "Surface Roughness Effects on Nosetip Ablation Characteristics," Paper 74-513, Palo Alto, Calif., 1974.